Supporting Information

Photovoltaic-Assisted Water Oxidation on $MoCoO_x$-Coupled Multi-Element-Doped $BiVO_4$ Photoanode Enabling 6.4% Unbiased Solar-to-Hydrogen Efficiency under Visible Light

Aditya Raj,[1] Munmun Majumder,[1] Arjun P B,[2] Dipanjan Maity,[3] Mukhesh K. Ganesha,[4] Ashutosh K. Singh,[4,5,6] Debasis De,[2,*] and Gobinda Gopal Khan [1,*]

[1] Department of Material Science and Engineering, Tripura University (A Central University), Suryamaninagar, Agartala, Tripura 799 022, India
[2] Rajiv Gandhi Institute of Petroleum Technology Bengaluru Campus, Kambalipura, Sulibele Hobli, Hosakote, Bengaluru 562 165, Karnataka, India
[3] Chemistry and Physics of Materials Unit, Jawaharlal Nehru Centre for Advanced Scientific Research, Jakkur, Bengaluru 560 064, India
[4] Centre for Nano and Soft Matter Sciences, Bangalore, Karnataka, 562162 India
[5] Academy of Scientific and Innovative Research (AcSIR), Ghaziabad- 201002, India.
[6] Manipal Academy of Higher Education, Manipal, Karnataka, 576104, India

Corresponding author e-mail: D. De: debasisd@rgipt.ac.in, debasis.ju@gmail.com, G G Khan: gobinda.gk@gmail.com, gobindakhan@tripurauniv.ac.in

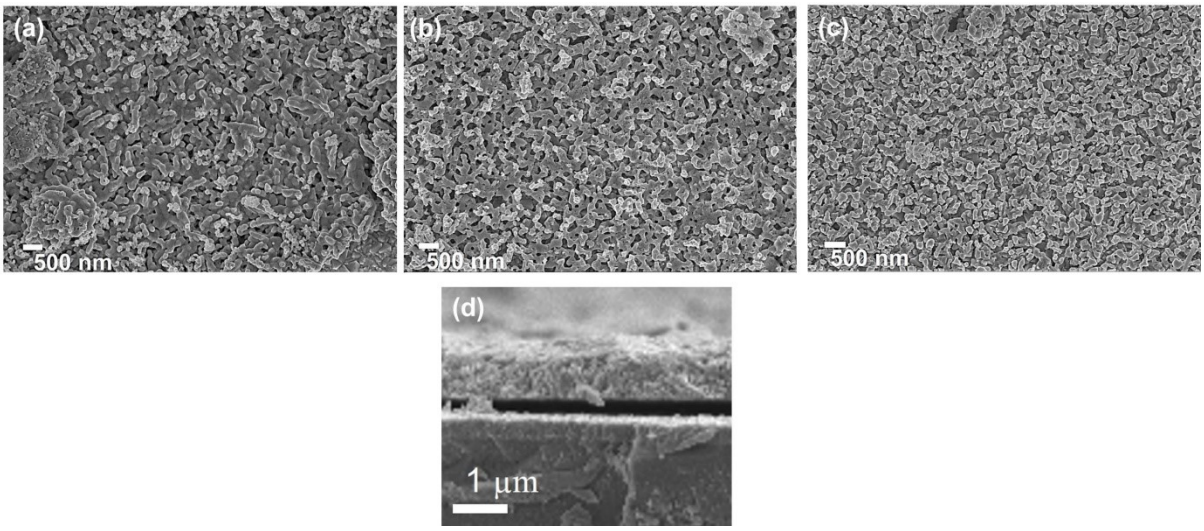

Figure S1. Low magnification FESEM images of (a) $BiVO_4$, (b) TiWP-$BiVO_4$, and (c) $MoCoO_x$/TiWP-$BiVO_4$ samples. (d) Cross-sectional FESEM of the optimal $MoCoO_x$/TiWP-$BiVO_4$ photoanode.

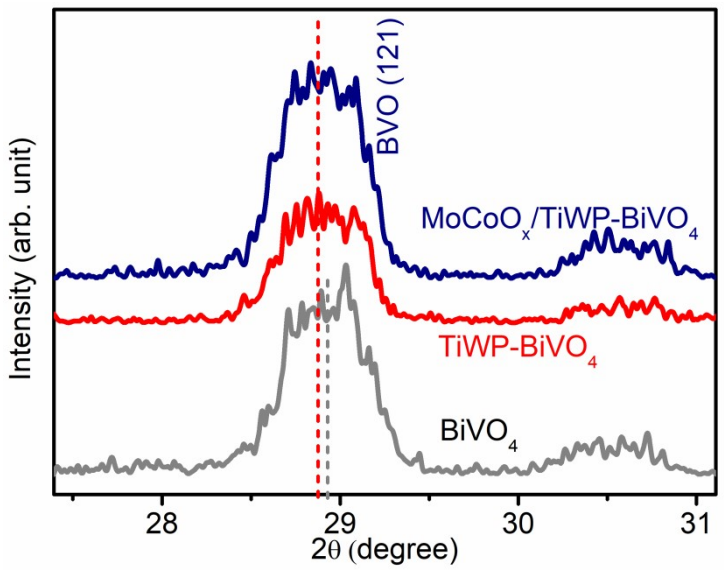

Figure S2. Magnified XRD patterns of the samples showing (121) crystallographic plane.

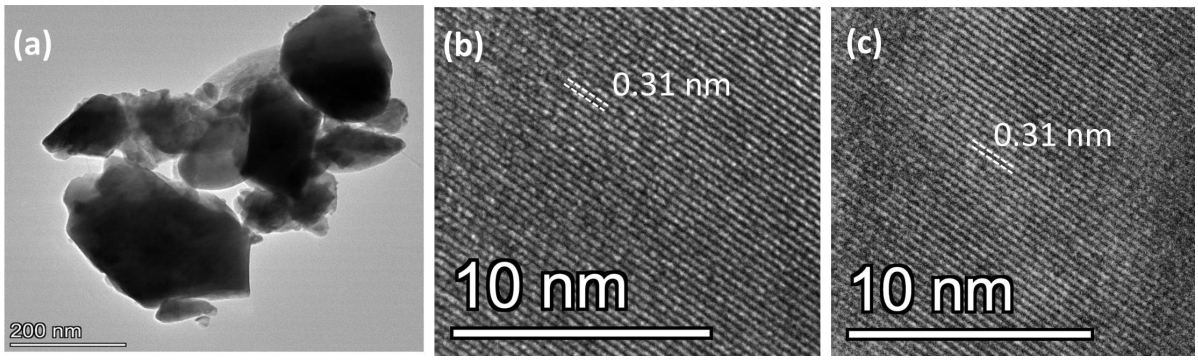

Figure S3. Low magnification TEM image of (a) $MoCoO_x/TiWP\text{-}BiVO_4$ sample. HRTEM images of (b) $BiVO_4$ and (c) $TiWP\text{-}BiVO_4$ photoanodes.

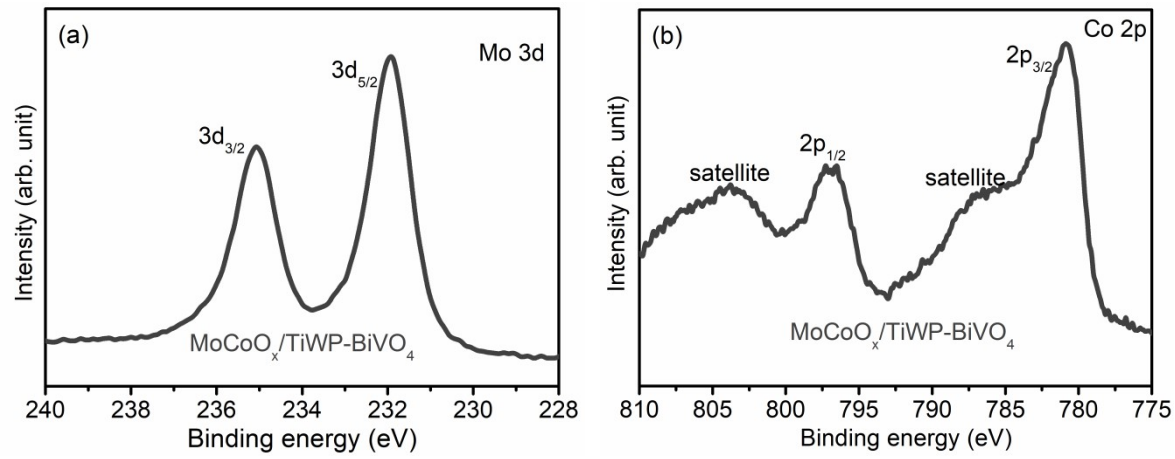

Figure S4. XPS spectrum of (a) Mo 3d and (b) Co 2p for $MoCoO_x$/TiWP-$BiVO_4$ sample.

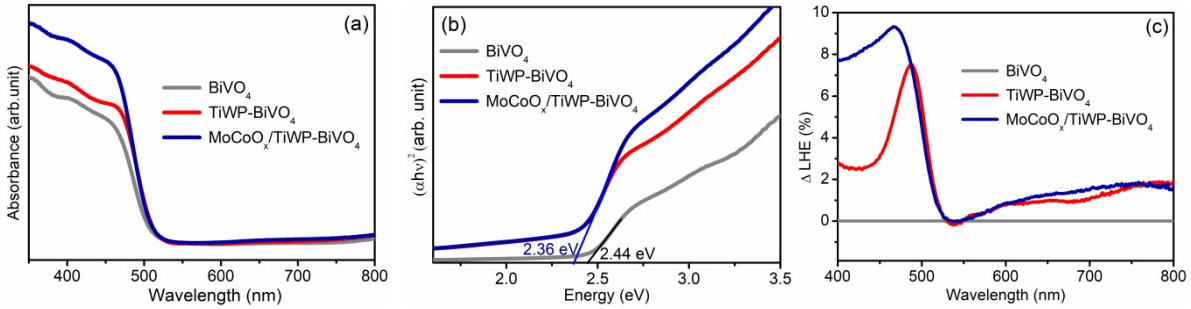

Figure S5. (a) UV-vis absorption spectra, (b) Kubelka-Munk plots, and (c) ΔLHE% plots for the samples.

Table S1: Information regarding synthesis of the best PEC performing (optimal) Ti, W, and P-doped $BiVO_4$ photoanodes:

Sample Name	**Basic solution used**	**Amount of $TiCl_3$ solution added**	**Amount of Sodium tungstate dehydrate added**	**Amount of triethyl phosphate added**	**Photocurrent density @1.23 V_{RHE} (mA/cm²)**
Pure $BiVO_4$	0.2 M $VO(acac)_2$ solution in 20 mL of DMSO	-	-	-	1.05
Ti (5µL) - $BiVO_4$	0.2 M $VO(acac)_2$ solution in 20 mL of DMSO	5 µL	-	-	3

Ti (10µL) - $BiVO_4$ ($Ti\text{-}BiVO_4$)	**0.2 M $VO(acac)_2$ solution in 20 mL of DMSO**	**10 µL**	**-**	**-**	**3.3**
Ti (15µL)-$BiVO_4$	0.2 M $VO(acac)_2$ solution in 20 mL of DMSO	15 µL	-	-	2.8
W (5.2 mM)-$BiVO_4$	0.2 M $VO(acac)_2$ solution in 20 mL of DMSO	-	5.2 mM	-	1.7
W (7.2mM)-$BiVO_4$ ($W\text{-}BiVO_4$)	**0.2 M $VO(acac)_2$ solution in 20 mL of DMSO**	**-**	**7.2 mM**	**-**	**1.8**
W(9.2mM)-$BiVO_4$	0.2 M $VO(acac)_2$ solution in 20 mL of DMSO	-	9.2 mM	-	1.6
P(5µL)-$BiVO_4$	0.2 M $VO(acac)_2$ solution in 20 mL of DMSO	-	--	5 µL	2.8
P (10µL)-$BiVO_4$ ($P\text{-}BiVO_4$)	0.2 M $VO(acac)_2$ solution in 20 mL of DMSO	**-**	**--**	10 µL	**3**
P (15µL)-$BiVO_4$	0.2 M $VO(acac)_2$ solution in 20 mL of DMSO	-	--	15 µL	2.9
TiP (5 µL) - $BiVO_4$	0.2 M $VO(acac)_2$ solution in 20 mL of DMSO	10 µL	--	5 µL	3.6

TiP (10 µL) - $BiVO_4$ **(TiP-$BiVO_4$)**	0.2 M $VO(acac)_2$ solution in 20 mL of DMSO	10 µL	--	10 µL	**3.7**
TiP (15 µL) - $BiVO_4$	0.2 M $VO(acac)_2$ solution in 20 mL of DMSO	10 µL	--	15 µL	3.5
TiW(5.2 mM)-$BiVO_4$	0.2 M $VO(acac)_2$ solution in 20 mL of DMSO	10 µL	5.2 mM	-	3.7
TiW (7.5 mM)-$BiVO_4$ **(TiW- $BiVO_4$)**	0.2 M $VO(acac)_2$ solution in 20 mL of DMSO	10 µL	7.5 mM	-	**3.9**
TiW (9.2 mM)-$BiVO_4$	0.2 M $VO(acac)_2$ solution in 20 mL of DMSO	10 µL	9.2 mM	-	3.6
TiWP (5 µL)-$BiVO_4$	0.2 M $VO(acac)_2$ solution in 20 mL of DMSO	10 µL	7.5 mM	5 µL	4.21
TiWP (10 µL)- $BiVO_4$ **(TiWP-$BiVO_4$)**	0.2 M $VO(acac)_2$ solution in 20 mL of DMSO	10 µL	7.5 mM	10 µL	**4.37**
TiWP (15 µL)- $BiVO_4$	0.2 M $VO(acac)_2$ solution in 20 mL of DMSO	10 µL	7.5 mM	15 µL	4.02

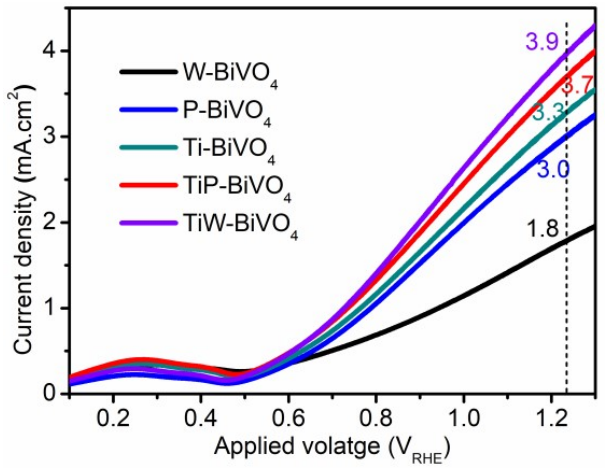

Figure S6. LSV profiles of the different elements (W, Ti, and P) doped optimized $BiVO_4$ samples, which exhibited the best PEC performance.

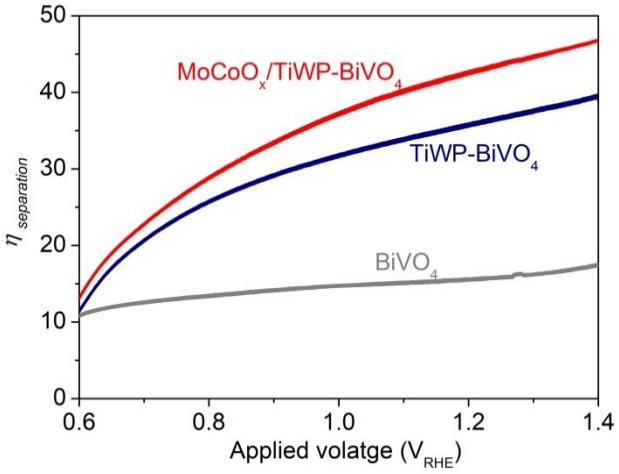

Figure S7. Charge-separation efficiency vs. voltage plots for the as-prepared photoanodes.

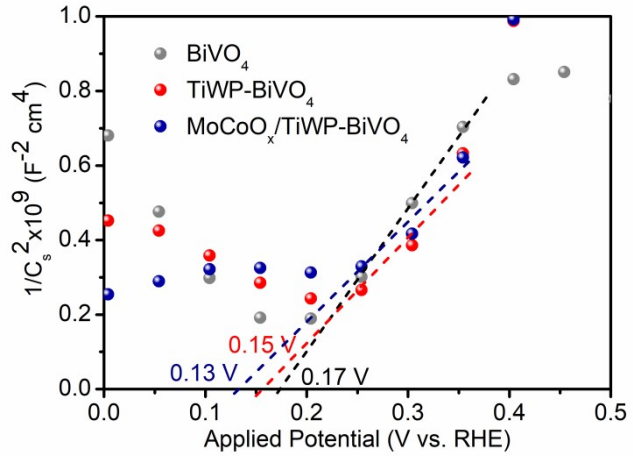

Figure S8. Mott–Schottky plots of the photoanodes at a low potential window.

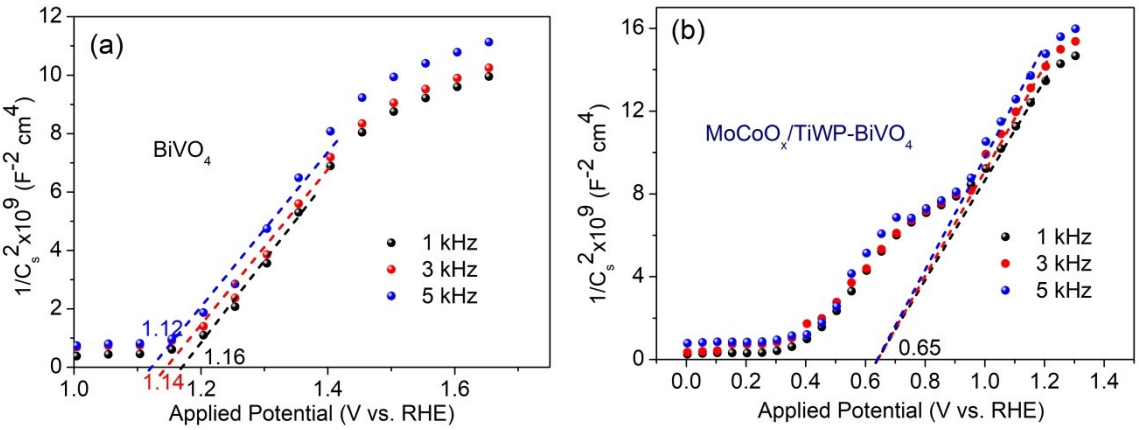

Figure S9. Frequency–dependent Mott–Schottky plots of the photoanodes.

The MS plots recorded over a range of frequencies (1, 3, and 5 kHz) reveal pronounced frequency dispersion in pristine $BiVO_4$ relative to $MoCoO_x$/TiWP-$BiVO_4$. For the pristine $BiVO_4$ photoanode, pronounced frequency dispersion in both the slope and the flat-band potential is observed, indicating substantial surface-state capacitance and Fermi-level pinning. In contrast, the $MoCoO_x$-modified TiWP-$BiVO_4$ electrode exhibits significantly reduced frequency dependence, demonstrating effective suppression of surface states. It is evident that $MoCoO_x$ modification de-pins the Fermi level and improves the band bending.

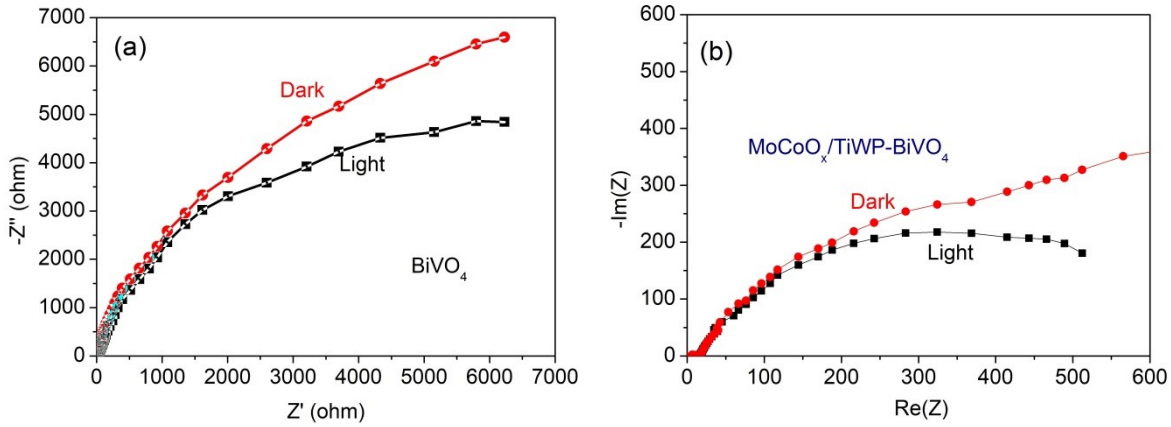

Figure S10. EIS spectra obtained at 1.23 V_{RHE} in the dark and under illumination.

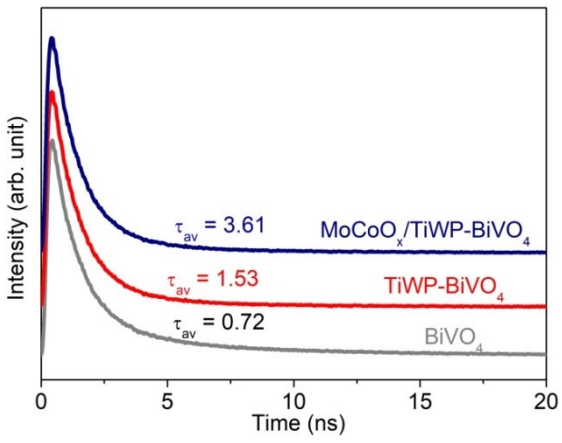

Figure S11. Time-resolved photoluminescence decay curves of the photoanodes.

Table S2. Fitted parameters of PEIS Nyquist plots (recorded at V= 1.23 V_{RHE}) for the photoanodes.

Photoanode	**R_s (Ω)**	**R_{ct} (Ω)**
$BiVO_4$	12.27	1027.4
TiWP-$BiVO_4$	10.87	96.51
$MoCoO_x$/TiWP-$BiVO_4$	9.64	64.42

Table S3. R_{ct} (Ω) values of the TiWP-$BiVO_4$ and $MoCoO_x$/TiWP-$BiVO_4$ photoanode recorded at different applied potentials.

V_{RHE} (V)	**R_{ct} (Ω)**	
	TiWP-$BiVO_4$	**MoCoOx/TiWP-$BiVO_4$**
1.23	96.51	64.42
0.9	112.10	79.21
0.6	129.62	91.34

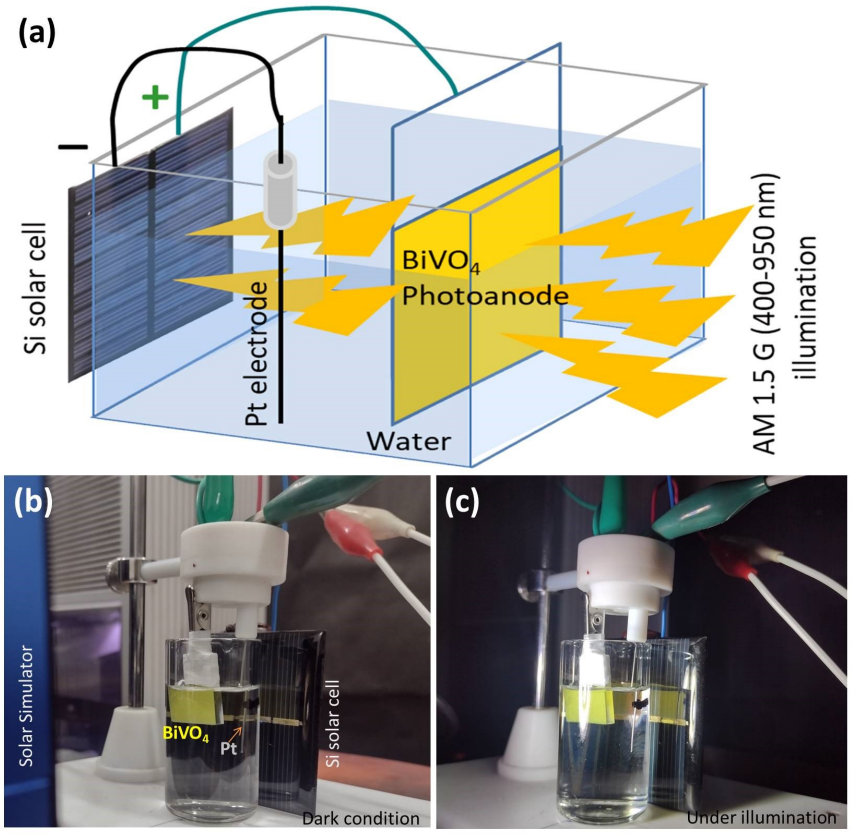

Figure S12. The PV-PEC tandem cell setup with $MoCoO_x$/TiWP-$BiVO_4$ photoanode and Si solar cell: (a) schematic diagram, photograph of the cell setup under dark (b) and light illumination (c) conditions.

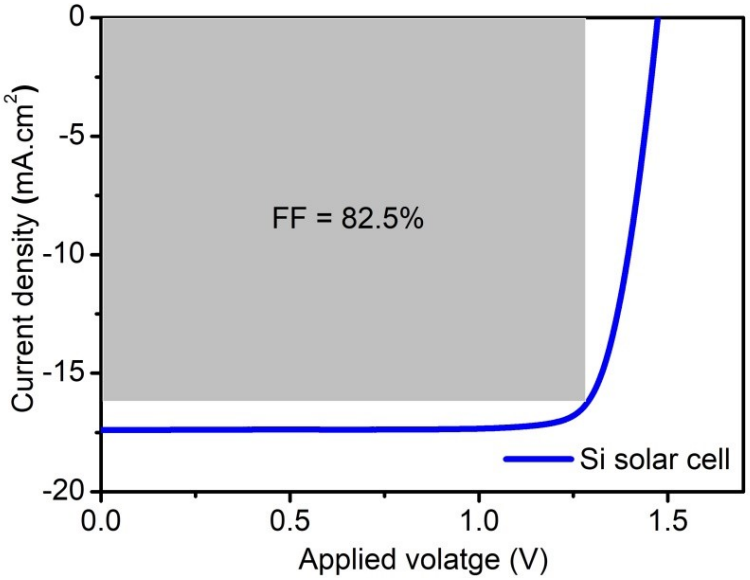

Figure S13. J-V curve of the commercial Si solar cell under AM 1.5 G radiation.

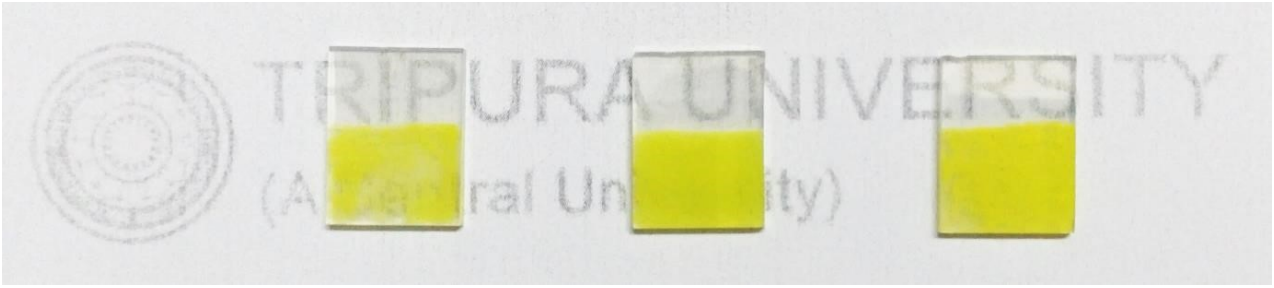

Figure S14. Photographs of the as-prepared $BiVO_4$, TiWP-$BiVO_4$, and $MoCoO_x$/TiWP-$BiVO_4$ photoanodes (left to right) after PEC studies.

Table S4. Comparison of the performance of different doped $BiVO_4$ photoanodes coupled with Co-based OECs.

Photoanode	**Photocurrent density (**mA cm^{-2}**) at 1.23 V_{RHE} (pH value)**	**Onset potential (V_{RHE})**	**Light source**	**ABPE(%)**	**STH(%)**
$MoCoO_x$/TiWP-$BiVO_4$[This work]	**4.75 (pH 7)**	**0.4**	AM 1.5 G, 100 mW. cm^{-2} visible light (400–950 nm)	**1.2**	6.4%
Co-Pi/N-$BiVO_4$[1]	3.7 (pH 7)	0.4	AM 1.5G, 100 mW cm^{-2}	1.16	0.14%
$FeCoO_x$/$BiVO_4$[2]	4.85 (pH 9.5)	0.4	AM 1.5G, 100 mW cm^{-2}	1.16	--
CoBi/Electrochemic	3.2 (pH 9.5)	0.35	AM 1.5G, 100 mW cm^{-2}	1.1	--

al- $BiVO_4$[3]					
CoPi/Gradient W:$BiVO_4$[4]	3.6 (pH 7.3)	-	AM 1.5G, 100 mW cm^{-2}	-	4.9%
$Co_3O_4/BiVO_4$[5]	2.71 (pH 7)	0.5	AM 1.5G, 100 mW cm^{-2}	-	--
Co-Pi/[001] $BiVO_4$[6]	6.1 (pH 7)	0.3	AM 1.5G, 100 mW cm^{-2}	-	--
CoPi/NiMoO4/$BiVO_4$[7]	5.3 (pH 6.4)	0.33	AM 1.5G, 100 mW cm^{-2}	1.18	--
FeNi(OH)x/CoPy/$BiVO_4$[8]	4.75 (--)	-	AM 1.5G, 100 mW cm^{-2}	1	--
CoPi/$V_{13}O_{16}$/ $BiVO_4$[9]	5 (pH 7)	0.37	AM 1.5G, 100 mW cm^{-2}	1.55	--
NiCo-LDH/$BiVO_4$[10]	3.4 (pH 7.3)	0.24	AM 1.5G, 100 mW cm^{-2}	0.66	--
$CoF_2/BiVO_4$ [11]	5.1 (pH 7)	0.3	AM 1.5G, 100 mW cm^{-2}	0.66	--
CoOOH/$BiVO_4$[12]	4 (pH 7)	0.25	AM 1.5G, 100 mW cm^{-2}	--	--
CoLa-LDH/ $BiVO_4$[13]	2.7 (pH 7)	0.19	AM 1.5G, 100 mW cm^{-2}	0.4	--
CoFe-H/$BiVO_4$[14]	2.48 (pH 7)	0.23	AM 1.5G, 100 mW cm^{-2}	--	--
NiO/CoOx/BiVO4 [15]	3.5 (pH 7)	0.3	AM 1.5G, 100 mW cm^{-2}	--	--
CoAl-LDH/Mo: $BiVO_4$ [16]	5.8 (pH 9.5)	0.26	AM 1.5G, 100 mW cm^{-2}	1.87	--
CoSn-LDH/GQDs/ $BiVO_4$[17]	4.15 (pH 11)	0.42	AM 1.5G, 100 mW cm^{-2}	1.26	--
$CoMoO_4/BiVO_4$[18]	3 (pH 6.8)	0.4	AM 1.5G, 100 mW cm^{-2}	--	--
N-CoFeOx/$BiVO_4$[19]	4.83 (pH 9.7)	0.36	AM 1.5G, 100 mW cm^{-2}	--	--
CoPi/WTi-$BiVO_4$[20]	2.4 (pH 7)	0.32	AM 1.5G, 100 mW cm^{-2}	--	--

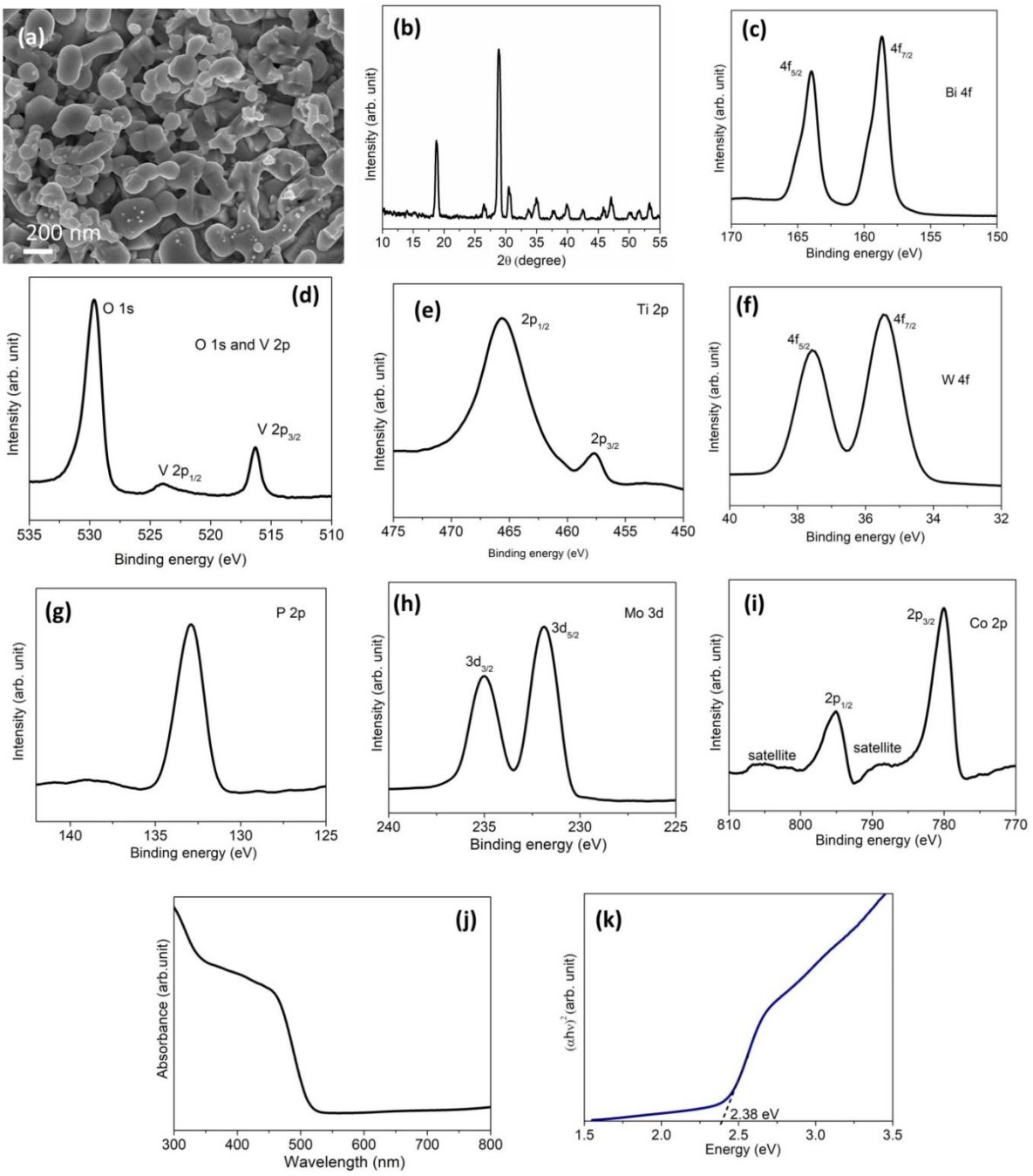

Figure S15. Characterization of the $MoCoO_x$/TiWP-$BiVO_4$ photoanode after 6 h of operation in the PV–PEC tandem device configuration: (a) FESEM image, (b) XRD pattern, XPS spectra of (c) Bi 4f, (d) V 2p and O 1s, (e) Ti 2p, (f) W 4f, (g) P 2p, (h) Mo 3d, and (i) Co 2p. The (j) UV-vis absorption spectrum and the (k) Kubelka-Munk plot.

References

1 X. Liang, P. Wang, F. Tong, X. Liu, C. Wang, M. Wang, Q. Zhang, Z. Wang, Y. Liu, Z. Zheng, Y. Dai and B. Huang, *Adv Funct Materials*, 2021, **31**, 2008656.

2 S. Wang, T. He, J. Yun, Y. Hu, M. Xiao, A. Du and L. Wang, *Adv Funct Materials*, 2018, **28**, 1802685.

3 S. Wang, P. Chen, J. Yun, Y. Hu and L. Wang, *Angewandte Chemie*, 2017, **129**, 8620–8624.

4 F. F. Abdi, L. Han, A. H. M. Smets, M. Zeman, B. Dam and R. Van De Krol, *Nat Commun*, 2013, **4**, 2195.

5 X. Chang, T. Wang, P. Zhang, J. Zhang, A. Li and J. Gong, *J. Am. Chem. Soc.*, 2015, **137**, 8356–8359.

6 H. S. Han, S. Shin, D. H. Kim, I. J. Park, J. S. Kim, P.-S. Huang, J.-K. Lee, I. S. Cho and X. Zheng, *Energy Environ. Sci.*, 2018, **11**, 1299–1306.

7 L. Gao, F. Li, H. Hu, X. Long, N. Xu, Y. Hu, S. Wei, C. Wang, J. Ma and J. Jin, *ChemSusChem*, 2018, **11**, 2502–2509.

8 X. Ning, B. Lu, Z. Zhang, P. Du, H. Ren, D. Shan, J. Chen, Y. Gao and X. Lu, *Angew Chem Int Ed*, 2019, **58**, 16800–16805.

9 H. Ren, T. Dittrich, H. Ma, J. N. Hart, S. Fengler, S. Chen, Y. Li, Y. Wang, F. Cao, M. Schieda, Y. H. Ng, Z. Xie, X. Bo, P. Koshy, L. R. Sheppard, C. Zhao and C. C. Sorrell, *Advanced Materials*, 2019, **31**, 1807204.

10 H. She, P. Yue, X. Ma, J. Huang, L. Wang and Q. Wang, *Applied Catalysis B: Environmental*, 2020, **263**, 118280.

11 B. Zhang, L. Chou and Y. Bi, *Applied Catalysis B: Environmental*, 2020, **262**, 118267.

12 F. Tang, W. Cheng, H. Su, X. Zhao and Q. Liu, *ACS Appl. Mater. Interfaces*, 2018, **10**, 6228–6234.

13 M. Chhetri, S. Dey and C. N. R. Rao, *ACS Energy Lett.*, 2017, **2**, 1062–1069.

14 W. Liu, H. Liu, L. Dang, H. Zhang, X. Wu, B. Yang, Z. Li, X. Zhang, L. Lei and S. Jin, *Adv Funct Materials*, 2017, **27**, 1603904.

15 M. Zhong, T. Hisatomi, Y. Kuang, J. Zhao, M. Liu, A. Iwase, Q. Jia, H. Nishiyama, T. Minegishi, M. Nakabayashi, N. Shibata, R. Niishiro, C. Katayama, H. Shibano, M. Katayama, A. Kudo, T. Yamada and K. Domen, *J. Am. Chem. Soc.*, 2015, **137**, 5053–5060.

16 Y. Zhong, C. Wu, X. Jia, S. Sun, D. Chen, W. Yao, H. Ding, J. Zhang and T. Ma, *Chemical Engineering Journal*, 2023, **465**, 142893.

17 S. Alam and M. Qureshi, *J. Phys. Chem. Lett.*, 2021, **12**, 8947–8955.

18 J. Du, X. Zhong, H. He, J. Huang, M. Yang, G. Ke, J. Wang, Y. Zhou, F. Dong, Q. Ren and L. Bian, *ACS Appl. Mater. Interfaces*, 2018, **10**, 42207–42216.

19 J. Lin, X. Han, S. Liu, Y. Lv, X. Li, Y. Zhao, Y. Li, L. Wang and S. Zhu, *Applied Catalysis B: Environmental*, 2023, **320**, 121947.

20 X. Zhao, J. Hu, B. Wu, A. Banerjee, S. Chakraborty, J. Feng, Z. Zhao, S. Chen, R. Ahuja, T. C. Sum and Z. Chen, *J. Mater. Chem. A*, 2018, **6**, 16965–16974.